Ahmad Paknejad
BEAMS Department,
Université Libre de Bruxelles,
50 F.D. Roosevelt Ave.,
B-1050 Brussels, Belgium
e-mail: ahmad.paknejad@ulb.ac.be

Guoying Zhao
BEAMS Department,
Université Libre de Bruxelles,
50 F.D. Roosevelt Ave.,
B-1050 Brussels, Belgium
e-mail: guoying.zhao@ulb.ac.be

Simon Chesné
LaMCoS, CNRS UMR5259,
INSA-Lyon,
University of Lyon,
Lyon, F-69621, France
e-mail: simon.chesne@insa-lyon.fr

Arnaud Deraemaeker
BATir Department,
Université Libre de Bruxelles,
50 F.D. Roosevelt Ave.,
B-1050, Brussels, Belgium
e-mail: aderaema@ulb.ac.be

Christophe Collette
BEAMS Department,
Université Libre de Bruxelles,
50 F.D. Roosevelt Ave.,
B-1050 Brussels, Belgium;
Department of Aerospace and
Mechanical Engineering,
Université de Liège,
Allée de la Découverte 9,
4000 Liège, Belgium
e-mail: ccollett@ulb.ac.be

Hybrid Electromagnetic Shunt Damper for Vibration Control

It has been shown that shunting electromagnetic devices with electrical networks can be used to damp vibrations. These absorbers have however limitations that restrict the control performance, i.e., the total damping of the system and robustness versus parameter variations. On the other hand, the electromagnetic devices are widely used in active control techniques as an actuator. The major difficulty that arises in practical implementation of these techniques is the power consumption required for conditioners and control units. In this study, robust hybrid control system is designed to combine the passive electromagnetic shunt damper with an active control in order to improve the performance with low power consumption. Two different active control laws, based on an active voltage source and an active current source, are proposed and compared. The control law of the active voltage source is the direct velocity feedback. However, the control law of the active current source is a revisited direct velocity feedback. The method of maximum damping, i.e., maximizing the exponential time-decay rate of the response subjected to the external impulse forcing function, is employed to optimize the parameters of the passive and the hybrid control systems. The advantage of using the hybrid control configuration in comparison with purely active control system is also investigated in terms of the power consumption. Besides these assets, it is demonstrated that the hybrid control system can tolerate a much higher level of uncertainty than the purely passive control systems.
[DOI: 10.1115/1.4048389]

Keywords: vibration damping, hybridization, smart structures, electromagnetic transducer

1 Introduction

Recently, the electromagnetic shunt damper has been proposed as a very simple and effective passive control technique. The key idea of this technique is to connect a capacitor of capacitance C and a resistor of resistance R to the electromagnetic transducer of inductance L to form a resonant RLC circuit. The absorber dissipates the vibrational energy by the resistor and its resonance is tuned close to the resonance of the primary system thanks to the tuned capacitor [1]. Many optimization methods have been proposed to optimize the parameters R and C. de Marneffe [2] optimized the parameters through the method of maximum damping and H_∞ minimization when the system is under base excitation. He has also compared the resonant RLC shunt with a resistive shunt. Inoue et al. [3] derived the optimal parameters by using the fixed point theory which was initially proposed by Den Hartog for the mechanical vibration absorber [4]. In Ref. [5], the optimal parameters have been obtained analytically using both the H_2 and H_∞ optimization methods which consist in minimizing the root-mean-square (RMS) vibration under random excitation and the peak amplitude in the frequency domain, respectively. Moreover, Zhu et al. [6] studied the analogy between the electromagnetic shunt damper and a tuned mass damper (TMD). Then, the optimal parameters of an electromagnetic shunt have been adapted from the optimal parameters of the TMD (obtained by Ormondroyd and Den Hartog [7]) by using an equivalent mass, stiffness and damping coefficient for the electromagnetic shunt damper. The main shortcoming of this method is that the optimal parameters can be used only when the equivalent mass ratio is small enough because a full dynamic analogy does not exist.

The passive electromagnetic shunt damper only works well when it is perfectly tuned based on the knowledge of the resonance frequency of the system. In order to maintain a control performance, adaptive techniques have been proposed to tune the RC shunt damper. The use of feedforward [8] and feedback [9] loops has been studied to online adapt both the shunt resistance and capacitance to ensure the tuned frequency of the vibration absorber tracks the excitation frequency. In Ref. [10], another adaptation strategies based on minimizing the RMS vibration and minimizing the phase difference between two measurable signals have been used.

The control performance of the passive electromagnetic shunt damper is limited by system's parameters like the mass and the stiffness of the primary system and the coupling constant as well as the inductance of the coil [11]. A popular method to enhance the control authority of the passive shunt is to use negative impedance which can be implemented actively [12–14]. Basically, the negative

Contributed by the Design Engineering Division of ASME for publication in the Journal of Vibration and Acoustics. Manuscript received October 2, 2019; final manuscript received July 27, 2020; published online September 28, 2020. Assoc. Editor: Alper Erturk.

 Copyright © 2020 by ASME

impedance, i.e., the resistance and/or inductance, cancels the transducer's inherent impedance and increases the control current which subsequently leads to a higher control authority. It has been also shown in Refs. [15,16] that this technique could be effective to improve the control authority of nonlinear electromagnetic shunt damper. However, the designed system suffers from the stability issue which occurs when the total impedance of the circuit becomes negative [17]. Indeed, a good vibration control can be realized by using the active control systems when the electromagnetic device is used as an actuator. For example, designs of positive position feedback (PPF) control based on maximum damping criterion [18] and H_∞ optimization [19] have been proposed and then validated experimentally using an electromagnetic transducer. Furthermore, because the transducer can be used as both actuator and sensor, an active impedance control system has been introduced by implementing a feedback loop between the coil terminal current and voltage of the device [20,21]. In order to simplify the implementation of the active control system by reducing the number of components in use, a technique of sensorless active shunt control has been also proposed for an inertial vibration absorption [22]. However, the better control performance always comes at the price of a high-energy consumption [23]. The hybrid control system may be an effective control configuration by combining the advantages of both active and passive control systems [24]. In other words, the active part of a hybrid system requires much less power than a similar purely active system, while providing better vibration suppression than the passive system alone. The other interesting objective of having hybrid control system is to ensure a fail-safe behavior [25]. It means that in the case of failure of the active portion of the hybrid control configuration, the passive control system still provides some amount of damping. Despite these interests, no one to the best of our knowledge has studied the hybridization of the passive electromagnetic shunt damper with an active control system for the purpose of vibration damping improvement.

It is worth pointing out that the electromagnetic transducer is exerted in two types of commercial actuators, i.e., the inertial actuator and the reactive actuator. The inertial actuator is a force actuator that is in parallel to a passive mount consisting of a reaction mass supported by a spring attached to a substructure. Its resonance frequency is much lower than the fundamental resonance frequency of the controlled structure due to a very low stiffness of its spring. This may results in high deflections of the proof mass [26]. Furthermore, a classical way, known as direct-velocity-feedback (DVF), to artificially increase the viscous damping is to derive the actuator with a signal proportional to the velocity of the substructure. However, the stability of the system is no longer guaranteed for high value of the feedback gain even when the sensor and actuator are collocated [27]. Unlike the inertial actuators where actuation force acts against the inertial mass, reactive actuators can be directly mounted on the ground because of no additional passive mount. Interestingly, such actuators do not suffer from the aforementioned limitations. Therefore, it is proposed to use a reactive actuator in this study.

In the literature, there are a number of studies on active-passive-hybrid-piezoelectric-networks (APPN). Agnes [28] proposed the concept of APPN and Tsai et al. [29] presented more insight and fundamental understandings to the APPN configuration. Basically, the APPN integrates piezoelectric shunt damping with an active voltage or charge source to improve the performance of the system [30]. It was shown in Ref. [31] that the APPN is an attractive configuration for the applications where minimizing the power consumption is critical. Morgan et al. [32] used active coupling feedback to enhance the electromechanical coupling of the transducer. In most studies about the APPN, a collocated piezoelectric sensor has been used to generate the feedback signal. However, Li et al. [33] employed a velocity feedback control for the application of the APPN by using a displacement sensor. The optimal values of the resistance and inductance could be quite different from those of the purely passive system in the case of APPN. Therefore, Tsai el al. [34] proposed a methodology to determine the optimal values of the resistor and inductor simultaneously with the control law. Furthermore, the multiple APPN has been also investigated to control of a quadrilateral plate [35] and a ring structure [36].

In the present study, the active-passive hybrid electromagnetic shunt damper is proposed. This paper is organized as follows. A purely passive electromagnetic shunt damper is studied and the parameters of the R and C are optimized according to the method of maximum damping in Sec. 2. Then in Sec. 3, the hybrid configuration is modeled by combining either active voltage source in series and current source in parallel with the designed RC circuit. The power that flows between the structure and the transducer due to the application of an active control system with an hybrid configuration is discussed in Sec. 4. Section 5 demonstrates the analysis of robustness for purely passive control system and both hybrid control configurations under the resonance frequency uncertainty. The conclusions are drawn in Sec. 6.

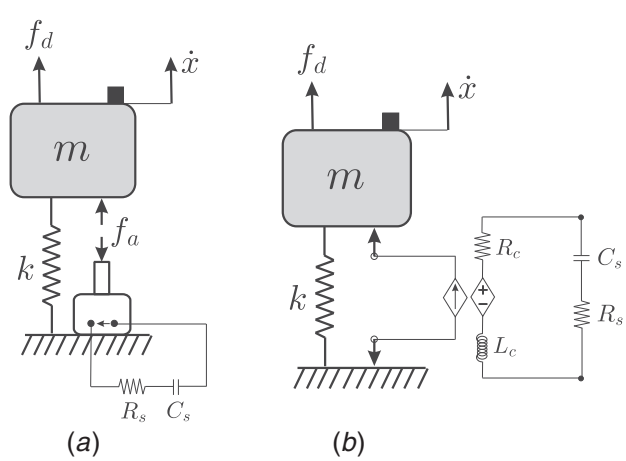

Fig. 1 Single-degree-of-freedom (SDOF) oscillator combined with the electromagnetic shunt damper: (*a*) mechanical model and (*b*) electrical equivalent model of the transducer

2 Passive Control System

Figure 1 shows the system under consideration. It is a SDOF oscillator with a mass m, spring k, and an electromagnetic device connected to a resistor of resistance R_s and a capacitor of capacitance C_s. The system is considered as an undamped SDOF when the electromagnetic transducer is in open-circuit condition. The system is excited by a disturbance force f_d, and the impulse response of the SDOF system is of interest. The electromagnetic device which is made of a permanent magnet and a coil has the following parameters: coupling constant T, coil inductance L_c, and coil resistance R_c. It can generate a force f_a which is proportional to the current I_t flowing inside the coil with a coupling coefficient T_i. In addition, the voltage across the transducer V is proportional to the velocity of the mass $\dot{x}$ with a coupling coefficient T_e. Both constants are equal to each other ($T_i = T_e = T$) due to a perfect transmission between the electrical and the mechanical energy. The coupling constant is equal to the product of the magnetic flux density B and the length of the coil seen by the magnetic flux [37], i.e., $T = 2\pi nrB$, where n and r are the number of turns in the coil and its radius (considering a cylindrical device), respectively. The governing equations of motion are written as:

$$m\ddot{x} + kx = f_d + f_a \tag{1a}$$

$$f_a = -TI_t = -T\dot{q} \tag{1b}$$

$$V = L\ddot{q} + R\dot{q} + \frac{1}{C}q = T\dot{x} \tag{1c}$$

where $L = L_c$, $C = C_s$, q is the charge flowing inside the coil. For the sake of simplicity, R is considered as the total resistance of the circuit, i.e., $R = R_c + R_s$ (Fig. 1(*b*)). The loop gain transfer function is now:

$$L(s) = A(s) \times B(s) = \frac{s}{m * s^2 + k} \times \frac{T^2 s}{Ls^2 + Rs + \frac{1}{C}} \tag{2}$$

where $A(s)$ and $B(s)$ are the sensor-actuator open-loop transfer function and the transfer function of the controller, respectively.

Equation (1) can be normalized with respect to the dimensionless time $\tau = \omega_0 t$ where $\omega_0 = \sqrt{k/m}$ as below:

$$x_1'' + x_1 = f - \beta_1 \omega_0 x_2' \tag{3a}$$

$$x_2'' + 2\xi\alpha x_2' + \alpha^2 x_2 = \beta_2/\omega_0 x_1' \tag{3b}$$

where the normalized parameters are as follows:

$$\begin{aligned} &\tau = \omega_0 t, \quad x_1(\tau) = x(t), \quad x_2(\tau) = q(t), \\ &\Omega = \omega/\omega_0, \quad f = \frac{1}{k} f_d, \quad \beta_1 = \frac{T}{k} \\ &\beta_2 = \frac{T}{L}, \quad \beta = \beta_1 \beta_2, \quad \omega_f = \frac{1}{\sqrt{LC}}, \\ &\alpha = \frac{\omega_f}{\omega_0}, \quad \xi = \frac{R}{2}\sqrt{\frac{C}{L}} \end{aligned} \tag{4}$$

The transfer function of the system from the normalized external force f to the normalized velocity of the mass $\dot{x}_1$ is then given by

$$\frac{\dot{x}_1}{f} = \frac{s(s^2 + 2\xi\alpha s + \alpha^2)}{(s^2+1)(s^2 + 2\xi\alpha s + \alpha^2) + \beta s^2} \tag{5}$$

where $s = j\Omega$ is the Laplace variable. In the remaining of the paper, the following numerical values are used: $m = 1$ kg, $k = 10^4$N/m, $T = 1$ N/Amp, and $L = L_c = 10^{-3}$ H. It should be mentioned that the resistance of the coil R_c is already included in R. According to Eq. (5), the passive control system adds another DOF to the system which makes the closed-loop response have two pairs. The root-locus of the system (Eq. (2)) is shown in Fig. 2 for

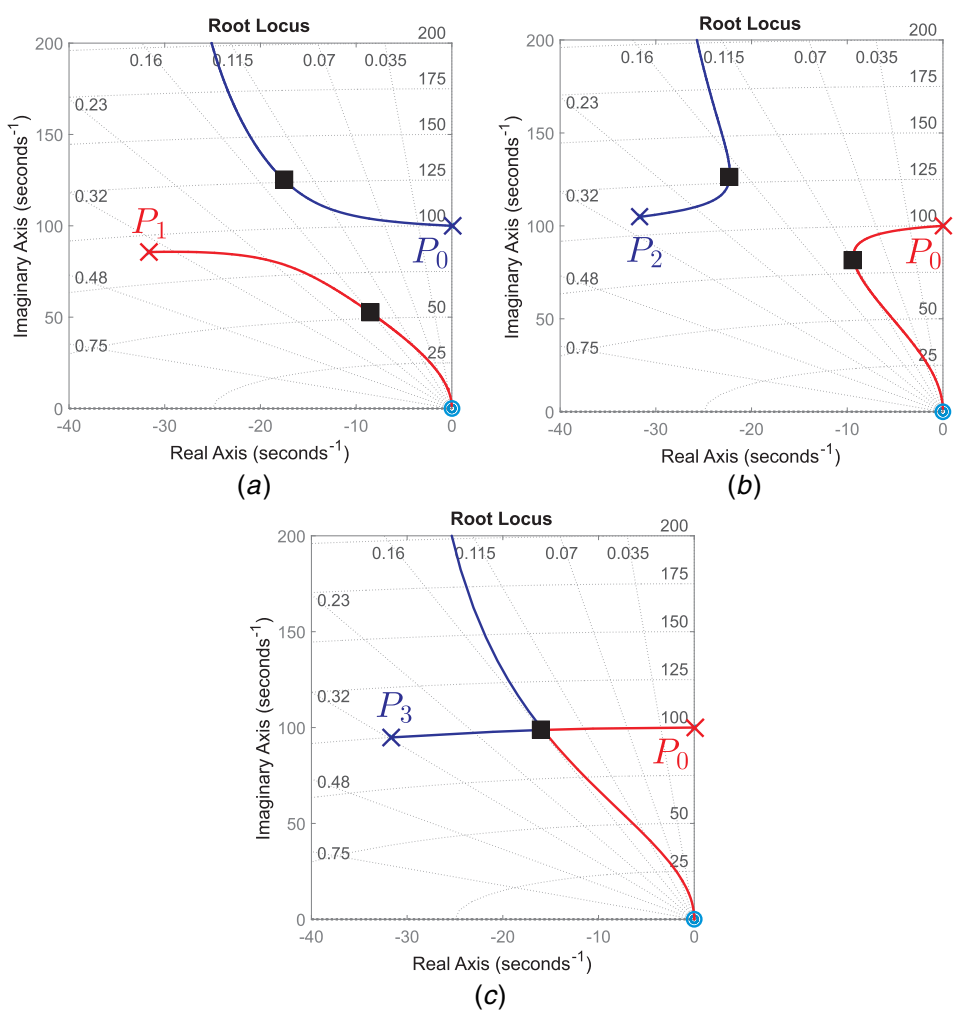

Fig. 2 Root-locus of the system shunted with the passive circuit and different values of the resistance *R* and capacitance *C* (P_0: pole of the primary system; P_1: pole of the controller using a higher value of *R* or a lower value of *C*; P_2: pole of the controller using a lower value of *R* or a higher value of *C*; P_3: pole of the controller using optimum values of the resistance and capacitance; ○: zero of the controller; ■: pole of the closed-loop system tuned based on the method of maximum damping)

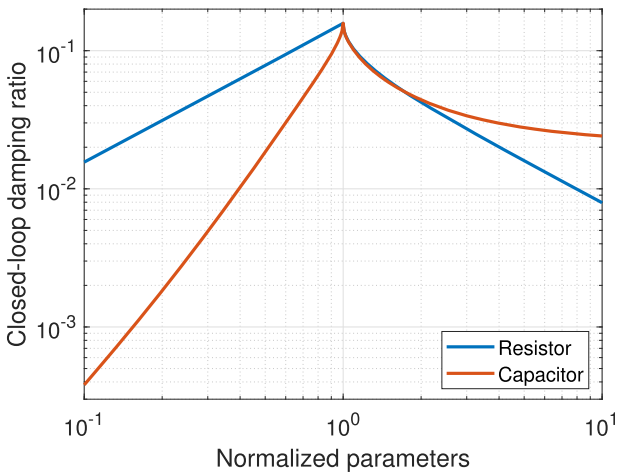

Fig. 3 Closed-loop damping ratio of the system against the variation of the shunt elements, i.e., resistance *R* and capacitance *C* normalized with respect to their optimal values

different values of the resistance R and the capacitance C. Basically, the locus consists of two loops starting from the pole of the primary system (P_0) and the pole of the resonant shunt (P_1 or P_2 or P_3), respectively. One of the loop goes to the origin and the other one goes to infinity. Considering the method of maximum damping, it can be observed that the maximum closed-loop damping can be realized when both loops are intersecting at one point (Fig. 2(*c*)). In other words, two closed-loop poles (■) are merged together. It is worth pointing out that the values of the R and C are taken arbitrarily to observe the different possible root locus curves. Considering the value of the resistance and capacitance corresponding to Fig. 2(*c*) as the optimum ones, Fig. 2(*a*) shows a typical root locus of the system when a higher value of the resistance or a lower value of the capacitance is taken. For a lower value of the resistance or a higher value of the capacitance, the typical root locus of the system is shown in Fig. 2(*b*).

The normalized transfer function, when two closed-loop poles are merged, can be simplified as

$$\frac{\dot{x}_1}{f} = \frac{s(s^2 + 2\xi\alpha s + \alpha^2)}{(s^2 + 2\eta\gamma s + \gamma^2)^2} \tag{6}$$

where η is the damping ratio, ω_c, and $\gamma = \omega_c/\omega_0$ are the resonance frequency and the normalized resonance frequency of the closed-loop response function, respectively. By matching the polynomial coefficients of the denominators of Eqs. (5) and (6), the set of equations can be obtained as follows:

$$4\eta\gamma = 2\xi\alpha \tag{7a}$$

$$4\eta^2\gamma^2 + 2\gamma^2 = \alpha^2 + \beta + 1 \tag{7b}$$

$$4\eta\gamma^3 = 2\xi\alpha \tag{7c}$$

$$\gamma^4 = \alpha^2 \tag{7d}$$

From Eqs. (7*a*), (7*c*), and (7*d*), it can be concluded that

$$\gamma_{opt} = \alpha_{opt} = 1 \tag{8}$$

which means that the optimal frequency of the circuit and the closed-loop resonance frequency of the system are equal to the resonance frequency of the primary system. Considering the above equation, η can be obtained as a function of ξ from Eq. (7*a*) ($\eta = 1/2\xi$). Substituting this equation and Eqs. (8) to (7*b*) yields:

$$\xi_{opt} = \sqrt{\beta} \tag{9}$$

As a consequence, the optimal parameters of resistance and capacitance can be obtained as follows:

$$C_{opt} = \frac{1}{L\omega_0^2} \tag{10a}$$

$$R_{opt} = \frac{2T}{\sqrt{kC_{opt}}} \tag{10b}$$

Figure 3 shows the closed-loop damping ratio of the system (Eq. (6)) against the variation of the resistance R and capacitance C, individually, normalized with respect to their optimal values. Note that one parameter is kept constant when the other one is varied. As it can be seen, the only values which can realize the maximum damping are only the optimal values.

Figure 4(*a*) shows the frequency response for five different values of the resistance R when the capacitance C is set to its optimal value and kept constant. All the curves are intersecting at two points which are called fixed points. For $R < R_{opt}$, two resonances appear in the vicinity of the resonance frequency of the primary system. The controller is no longer effective in the terms of amplitude reduction when $R \to 0$. In addition, the performance degradation can also be observed when $R > R_{opt}$. Especially when $R \to \infty$, the controlled system acts like a primary system with no additional damping. By using the method of maximum damping

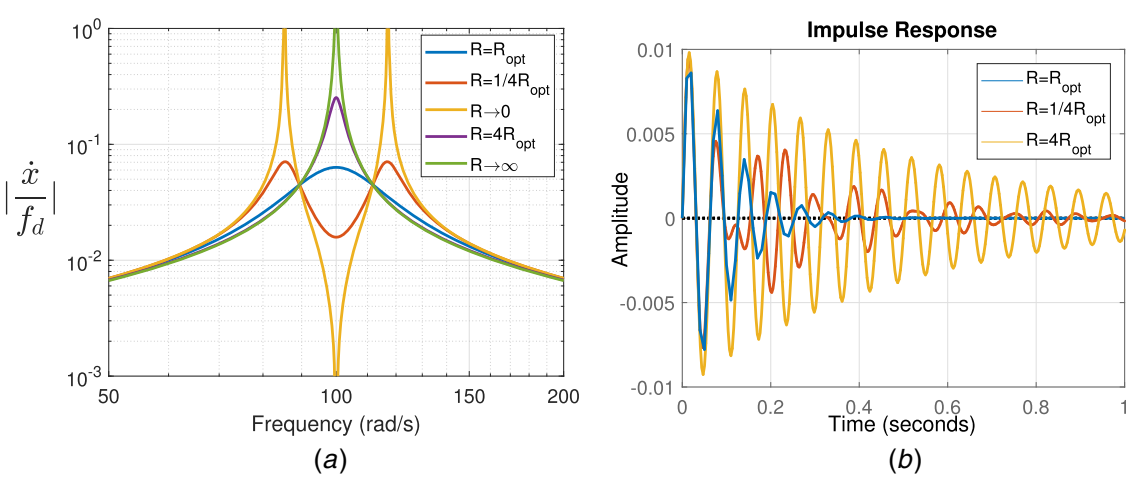

Fig. 4 For the attached passive *RC* circuit: (*a*) frequency response as well as (*b*) the impulse response for different values of *R*

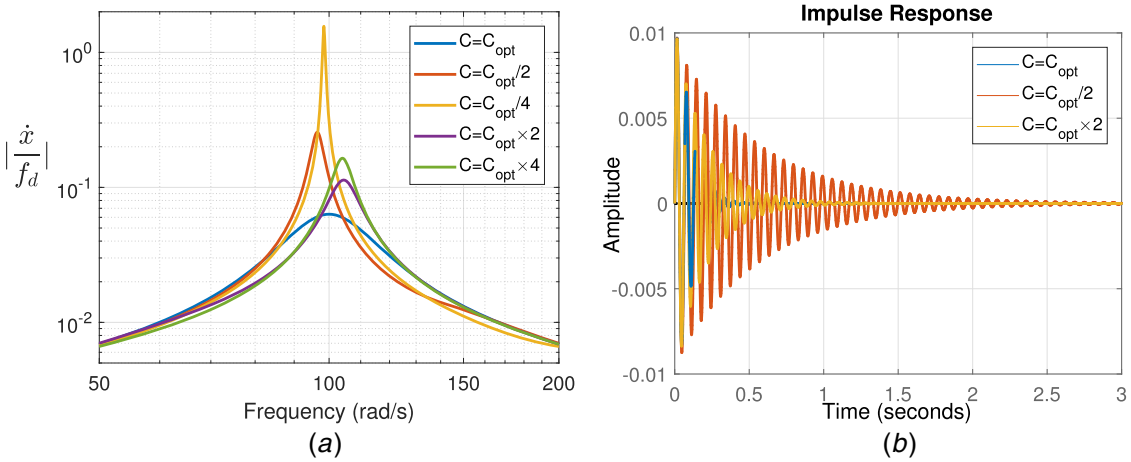

Fig. 5 For the attached passive *RC* circuit: (*a*) frequency response as well as (*b*) the impulse response for different values of *C*

to optimize the parameters of the controller, the settling time of the transient response of the system to the impulse disturbance should be minimized. To verify this fact, the impulse response in the time domain is also shown in Fig. 4(*b*) for three different values of R. As it can be seen, the minimum settling time can be achieved by considering the designed optimal value of R obtained in Eq. (10*b*).

Figure 5(*a*) shows the frequency response for five different values of the capacitance C. Note that the value of R is set to its optimum and kept constant. The evidence of the performance degradation can be seen by a deviation from the optimal capacitance C_{opt}. It is wroth pointing out that the amplitude of the resonance exhibits one peak when the parameters are optimally tuned according to Eq. (10). However, mistuning leads to the increase of one peak accompanied by the reduction of the other one. Figure 5(*b*) also demonstrates the impulse response of the system for three different values of the capacitance C. Minimum settling time occurs only when the capacitance is set to its optimum.

Consequently, the passive shunt system as a frequency dependent control system is less robust to resonance uncertainty. Some studies have introduced different strategies to online adapt the parameters of the passive shunt to ensure the tuned frequency of the vibration absorber tracks the excitation frequency. More details are presented in Refs. [8,9]. An alternative solution to online adaptation is to employ a broadband vibration absorber such that the system can tolerate a high level uncertainty, which is of interest in the present work. In the next sections, we propose two different hybrid control systems based on active voltage and current sources. One of the advantage of the proposed hybrid system is to make the system robust to resonance uncertainty.

3 Hybrid Control System

From Eqs. (7)–(9) and (4), it can be concluded that the optimal closed-loop damping is $\eta_{opt} = T/(2\sqrt{kL})$. This shows that the stiffness of the structure as well as the coupling constant and the inductance of the transducer limit the maximum achievable damping obtained by the passive control system. Therefore, one method to enhance the control authority of the passive shunt is to use a negative inductance to artificially reduce the inductance of the circuit and subsequently increase the maximum achievable damping ratio. However, the closed-loop system is conditionally stable [12–14]. What follows is the study of using active control to improve the control performance of the passive electromagnetic shunt damper in terms of the closed-loop damping and the robustness to resonance uncertainty.

In the present study, two different configurations for the hybridization of the passive resonant shunt with an active control are considered (Fig. 6). In the first configuration shown in Fig. 6(*a*), the electromagnetic transducer is connected in series with *RC* elements and an active voltage source. The active voltage source is proportional to the velocity of the structure. The total voltage across the transducer (V) is then obtained by the summation of the active input voltage (V_{in}) and the voltage across the *RLC* circuit. Furthermore in the second configuration shown in Fig. 6(*b*), the electromagnetic transducer is connected in series with the *RC* circuit, and the active current source is in parallel with the shunting elements. Considering this configuration, the total current flowing in the transducer (I_t) is given by the algebraic sum of the input active current (I_{in}) and the current flowing inside the *RC* shunt circuit ($I_s = \dot{q}$) like $I_t = I_s - I_{in}$.

3.1 Hybridization With An Active Voltage Source. Considering the active voltage source, the electrical portion of the governing equations is modified as

$$L\ddot{q} + R\dot{q} + \frac{1}{C}q + V_{in} = T\dot{x} \tag{11a}$$

$$V_{in} = -g_1 T\dot{x} \tag{11b}$$

By substituting Eq. (11*b*) into Eq. (11*a*), it can be seen that the active voltage source directly affects the effective coupling constant of the transducer. Therefore, the actuator force is proportional to the current with a new coupling constant T^*. It is assumed that the transducer is ideal and there is a perfect balance between the electrical energy and the mechanical energy which means that there is no energy to be stored in the transducer [37]. According to the energy conservation principle [38], the variation of the stored energy is the sum of the external power input and the internal power generation. This concept can be written for the electromagnetic transducer in the presence of the active voltage source when there is no shunt as follows:

$$dW = Vdq + f_a dx = T(1+g_1)\frac{dx}{dt}idt + T^* idx \tag{12}$$

where d and W are the differential operator and the stored energy, respectively. By equating the above equation to zero, T^* can be obtained as follows:

$$T^* = T(1+g_1) \tag{13}$$

Figure 7 shows the root locus of the system, shunted with a *RC* circuit and the active voltage source in series, for the variation of feedback gain g_1. One sees that the system is stable because the

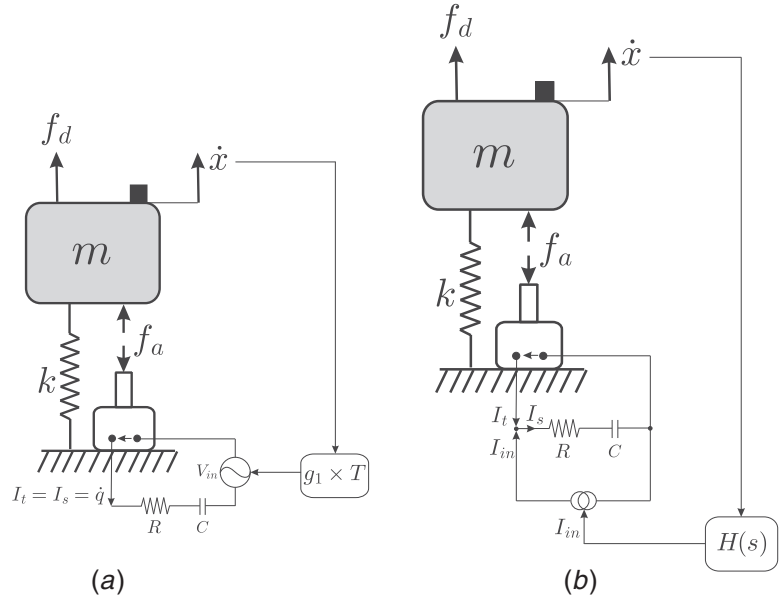

Fig. 6 Schematic of a SDOF oscillator attached to an hybrid control system consisting of an electromagnetic transducer connected to the passive *RC* shunt (*a*) in series with an active voltage source and (*b*) in parallel with an active current source

poles are always placed in the left half plane of the locus for all values of the feedback gain g_1. The locus has two complex poles and two zeros at the origin. By increasing the value of the feedback gain g_1, one pole goes toward the origin and the other one goes to infinity. It makes the system have two different resonances in the vicinity of the primary ones with the lower values of the damping than the damping of the passive control system. According to Eq. (10*b*), the optimal values of the resistance R is proportional to the coupling constant of the transducer. Considering the new constant of the transducer (Eq. (28)), the optimal value of the resistance can be modified as follows:

$$R^*_{opt} = \frac{2T}{\sqrt{kC_{opt}}}(1 + g_1) \tag{14}$$

Figure 8(*a*) compares the frequency response of the system with the passive control system combined with the active voltage source for two different values of the feedback gain g_1. For each value of g_1, the result is shown with and without correction of the resistance R according to Eqs. (14) and (10*b*), respectively. By updating the value of the resistance in this case, more energy can be dissipated in the resistor which leads to increase the damping of the system. A larger value of resistance is required by the application of the active voltage source than the purely passive system. In order to have a fail-safe and optimum design, the value of resistance should be changed to the lower one when the active control is turned off. For a specific value of the feedback gain g_1, the impulse response is shown in Fig. 8(*b*) when the value of the resistance R is modified based on Eq. (14). It can be seen that the exponential time-decay rate is maximized by updating the value of the resistance.

Similar studies have been already published for piezoelectric transducers when an active control is used to enhance the electromechanical coupling constant and subsequently improve significantly the passive piezoelectric shunt damping [30,32,34].

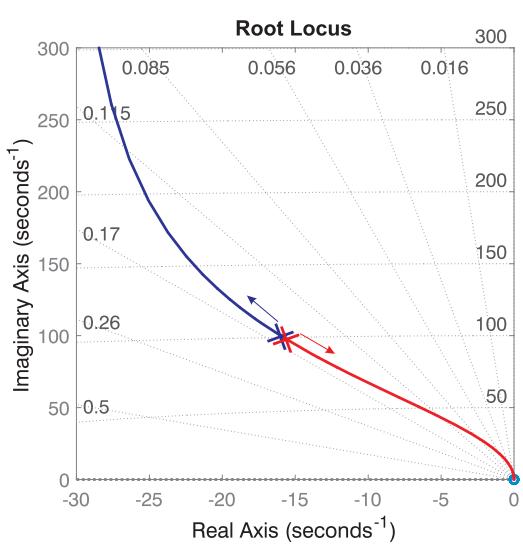

Fig. 7 Root-locus of the system shunted with *RC* circuit combined with active voltage source

3.2 Hybridization With An Active Current Source. In the previous section, we could see that the performance is increased when the resistance of the passive shunt elements changes in proportion to the enhanced coupling constant. In this case (i.e., increased value of the resistor), the system has a weak fail-safe behavior because the passive control system is not optimally tuned when the active voltage source is turned off. More details on the performance degradation of the passive control system in terms of both magnitude of response and time decay rate can be seen in Fig. 6 when a higher value of the resistance is chosen. What follows is the study of the hybrid control system using an active current source.

The equations of motion with the application of the active current source read:

$$m\ddot{x} + kx = f_d + f_a \tag{15a}$$

$$f_a = -TI_t = -T(\dot{q} + I_{in}) \tag{15b}$$

$$V = L(\ddot{q} + \dot{I}_{in}) + R\dot{q} + \frac{1}{C}q = T\dot{x} \tag{15c}$$

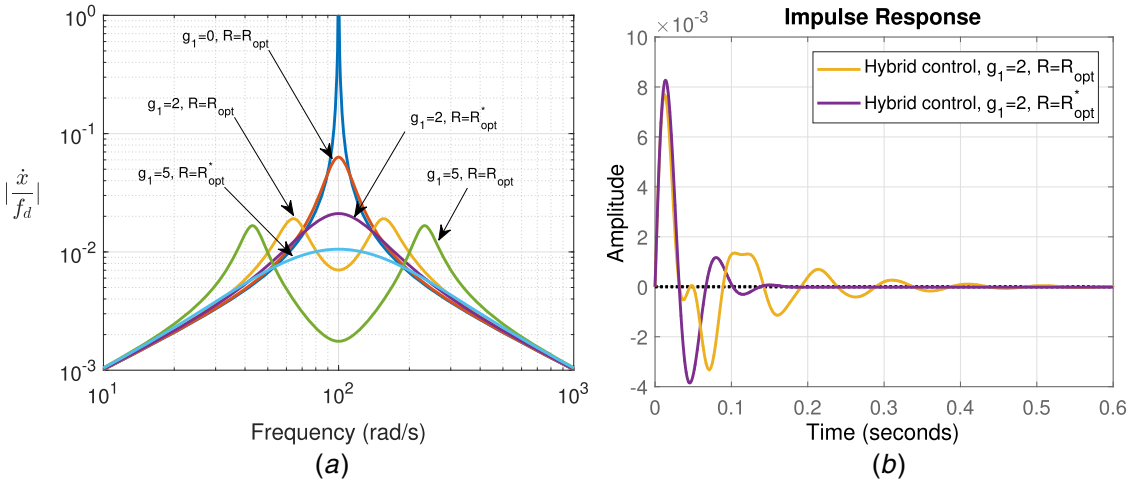

Fig. 8 With the application of the passive control system combined with the active voltage source: (*a*) the frequency response of the system for different values of the feedback gain g_1 as well as the resistance R and (*b*) the impulse response with and without the correction of the resistance R

The transfer function of the system from the active current (I_{in}) to the velocity of the mass ($\dot{x}$) is obtained as follows:

$$G(s) = \frac{\dot{x}}{I_{in}} = \frac{T(Rs + \frac{1}{C})}{(ms^2 + k)\left(Ls^2 + Rs + \frac{1}{C}\right) + T^2 s^2} \tag{16}$$

The root locus of the system, i.e., $G(s)H(s)$ when direct velocity feedback ($H(s) = -g_2/T$) is used as the active control law is shown in Fig. 9(*a*) for the variation of the feedback gain. It can be seen that even for low gains, the root locus passes through the imaginary axis and can create instabilities. This is due to the absence of a zero between the pole of the passive shunt damper and the primary pole of the structure which are placed right next to each other. A simple alternative control law is proposed to ensure the stability of the closed-loop system. The controller is still using the absolute velocity of mass, however, the filter is now defined as follows:

$$H(s) = -g_2 \frac{Ls^2 + Rs + \frac{1}{C}}{T\left(Rs + \frac{1}{C}\right)} \tag{17}$$

The real pole of the controller cancels the zero of the loop gain ($G(s)H(s)$) and the pair of complex zeros interacts with the pole of the system. The system is unconditionally stable by the application of the active current source because the closed-loop poles are always in the left half plane. Notice that, in order to avoid a constant component in the feedback loop, a high pass filter at very low frequency and a low pass filter at very high frequency should be added to the controller. These filters do not change the controller behavior for the flexible modes. When the feedback gain g_2 is zero, both poles of the system are placed right at the same locations thanks to the optimally design of the passive control system (Sec. 3). By increasing the feedback gain, the closed-loop damping ratio also increases. One of the pole moves on the upper branch and the other one moves on the lower branch. According to the method of maximum damping, the optimal feedback gain g_2^{opt} can be obtained when the two loops are intersecting at point "A" which is shown in

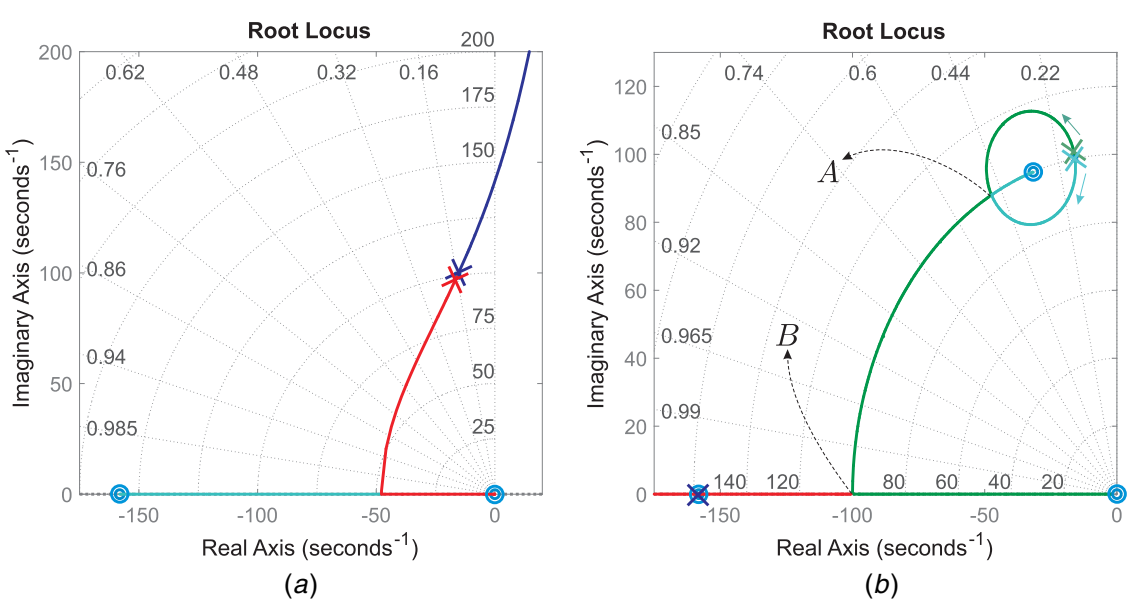

Fig. 9 Root-locus of the system shunted with *RC* circuit combined with active current source using (*a*) direct velocity feedback ($H(s) = g_2/T$) or (*b*) Eq. (17) for the active control law

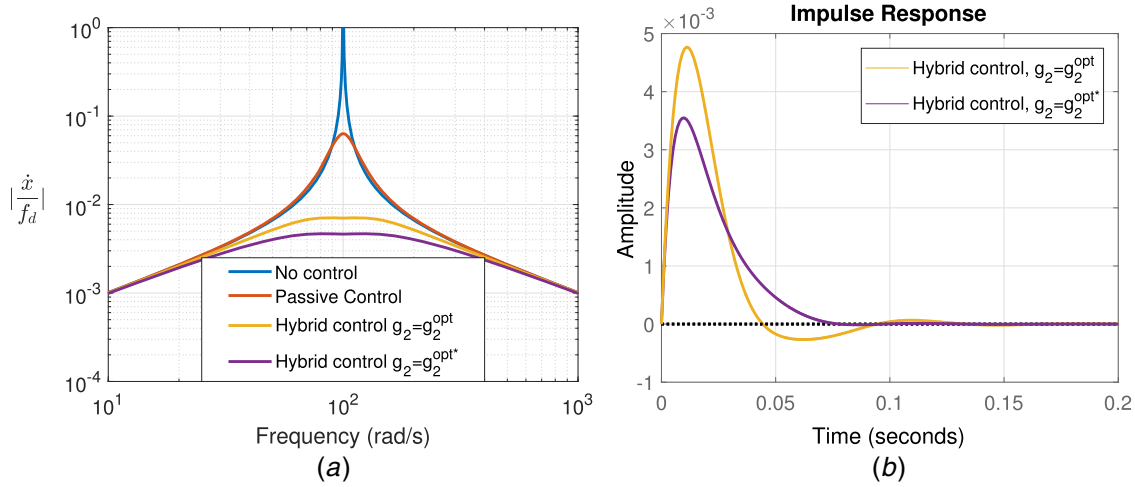

Fig. 10 With the application of the passive control system combined with the active current source: (*a*) the frequency response and (*b*) the impulse response of the system for two different values of the feedback gain g_2

Fig. 9(*b*). Considering $\lambda = g_2\omega_0/k$, the closed-loop transfer function from the normalized disturbance force f to the normalized velocity $\dot{x}_1$ is obtained as follows:

$$\frac{\dot{x}_1}{f} = \frac{s(s^2 + 2\sqrt{\beta}s + 1)}{(s^2 + \lambda s + 1)(s^2 + 2\sqrt{\beta}s + 1) + \beta s^2} \tag{18}$$

When the two poles of the system have the same damping μ and normalized resonance frequency δ, the closed-loop transfer function can be re-written as follows:

$$\frac{\dot{x}_1}{f} = \frac{s(s^2 + 2\sqrt{\beta}s + 1)}{(s^2 + 2\mu\delta s + \delta^2)^2} \tag{19}$$

The following equations are obtained by equating the polynomial coefficients of the denominator of the fraction on the right-hand side of Eqs. (18) and (19):

$$4\mu\delta = 2\sqrt{\beta} + \lambda \tag{20a}$$

$$4\mu^2\delta^2 + 2\delta^2 = 2\sqrt{\beta}\lambda + \beta + 2 \tag{20b}$$

$$4\mu\delta^3 = 2\sqrt{\beta} + \lambda \tag{20c}$$

$$\delta^4 = 1 \tag{20d}$$

The optimal value of the normalized tuning frequency δ is obtained from Eq. (20*d*) as

$$\delta_{opt} = 1 \tag{21}$$

which shows that the closed-loop system has the same resonance frequency as the resonance frequency of the primary one. The optimal value of the normalized feedback gain can be realized by substituting the damping ratio μ obtained from Eqs. (20*a*) and (21) into Eq. (20*b*):

$$\lambda_{opt} = 4\sqrt{\beta} \tag{22}$$

which yields:

$$g_2^{opt} = 4\frac{T}{\omega_0}\sqrt{\frac{k}{L}} \tag{23}$$

It should be mentioned that the parameters of the passive *RC* circuit do not change. This results in a perfect fail-safe behavior because the passive control system is still optimally tuned to provide η_{opt} damping when there is no active current in the actuator. Figure 10(*a*) compares the frequency response of the passive control system combined with the active current source for two different values of the feedback gain g_2. The optimal value is first used for the feedback gain $g_2^{opt} = 126.49$ (shown as point "A" in Fig. 9(*b*)), and then, it is increased to $g_2 = 200$ when a closed-loop pole touches the real axis (shown as point "B" in Fig. 9(*b*)) and the other one merges with the zero. In this case, the zero cancels one of the poles and the other one adds damping to the system. This gain ($g_2^{opt*} = 200$) can be defined as the second optimal value. Although it might slightly improve the settling time (Fig. 10(*b*)) in comparison with the one corresponding to the first optimal value, the power consumption will drastically increase (more details will be discussed in the next section) and the actuator might be saturated. For more than this value of the gain, the settling time is no longer minimized although it might realize lower magnitude of response than the magnitude of response obtained with the optimal values of the feedback gain. It should be mentioned that the active current source behaves like a direct-velocity-feedback (DVF) which is able to damp several modes as well. This topic is proposed for future studies.

In the present study, the ideal voltage and current sources have been considered to build the hybrid configurations. Basically, an ideal voltage source is supposed to have no internal impedance and an ideal current source is supposed to have an infinite internal impedance [39]. However, this is not the case for practical voltage and current sources. Therefore, the internal impedance of the sources can change the total impedance of the shunt when the active control is turned off. This may result in a problem in fail-safe behavior for practical implementation of the hybrid control system. This will be more discussed in the future works.

4 Powerflow Analysis

In the previous section, it has been shown that the hybrid control system can improve the control performance of the system in terms of the amplitude of response at the resonance frequency. A question may arise here is what is the main advantage of using a hybrid control system compared to a purely active control system. To answer this question, it is proposed to analyze the powerflow between the device and the primary structure due to the fact that an active control system requires an external power source for its operation. The power which flows at the interface of the structure and the actuator device can be written as follows:

$$P(s) = F_{aa}(j\omega) \times \dot{x}^*(j\omega) \tag{24}$$

Table 1 The expressions for G_f and G_{cl} for different control configurations

Parameters	G_{cl}	G_f
Hybrid control-voltage source	$\dfrac{(j\omega)(-L\omega^2+\left(1+g_1)Rj\omega+\dfrac{1}{C}\right)}{(-\omega^2+k)\left(-L\omega^2+(1+g_1)Rj\omega+\dfrac{1}{C}\right)-(g_1+1)^2T^2\omega^2}$	$-\dfrac{g_1(g_1+2)T^2(j\omega)}{-L\omega^2+(1+g_1)Rj\omega+\dfrac{1}{C}}$
Hybrid control-current source	$\dfrac{(j\omega)\left(-L\omega^2+Rj\omega+\dfrac{1}{C}\right)}{(-\omega^2+g_2j\omega+k)\left(-L\omega^2+Rj\omega+\dfrac{1}{C}\right)-T^2\omega^2}$	$-g_2$
DVF	$\dfrac{j\omega}{-\omega^2+g_3j\omega+k}$	$-g_3$

where P, F_{aa}, and $\dot{x}$ are the power, the control force applied by the active control system, and the velocity of the mass, respectively. The superscripts "*" represents the complex conjugate transpose. The real part of P is called the active power which corresponds to the dissipative behavior and the imaginary part is named the reactive power which corresponds to the energy exchanging between the device and the structure [40]. The average active power P_{ac} and the reactive power P_{re} can be written as follows:

$$P_{ac}=\frac{1}{2}\mathcal{R}(P(j\omega))=\frac{f_d^2}{2}\mathcal{R}(G_f(j\omega)\times G_{cl}(j\omega)\times G_{cl}^*(j\omega)) \tag{25a}$$

$$P_{re}=\frac{1}{2}\mathcal{L}(P(j\omega))=\frac{f_d^2}{2}\mathcal{L}(G_f(j\omega)\times G_{cl}(j\omega)\times G_{cl}^*(j\omega)) \tag{25b}$$

where $G_f(j\omega)$ and $G_{cl}(j\omega)$ are the frequency response function from the velocity of the structure to the control force and the frequency

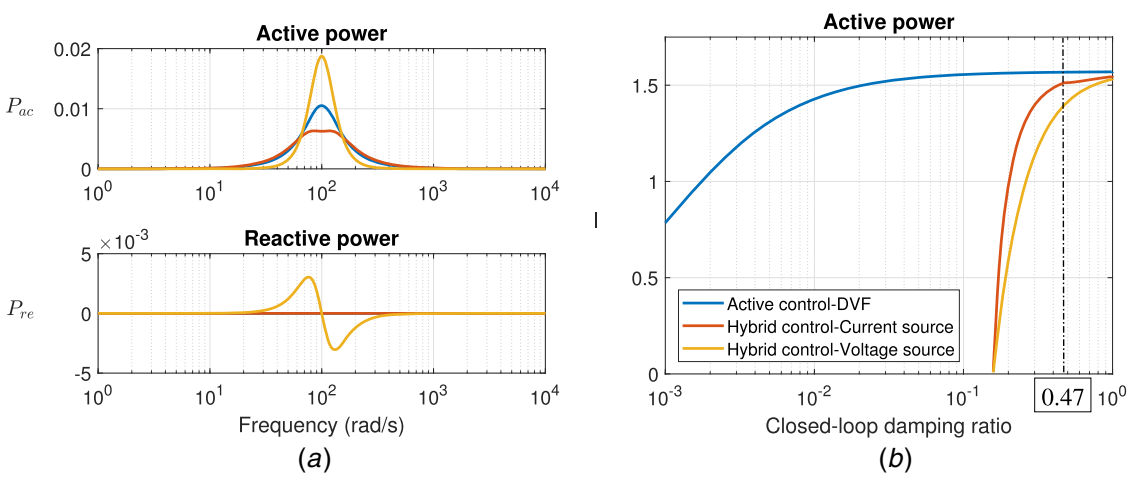

Fig. 11 Comparison between the purely active control system (DVF) and the hybrid control systems: (*a*) active and reactive power for a specific closed-loop damping ratio (=47%) and (*b*) the normalized mean square value of the active power *I* versus the closed-loop damping ratio (dash-dotted line shows the 0.47 damping ratio)

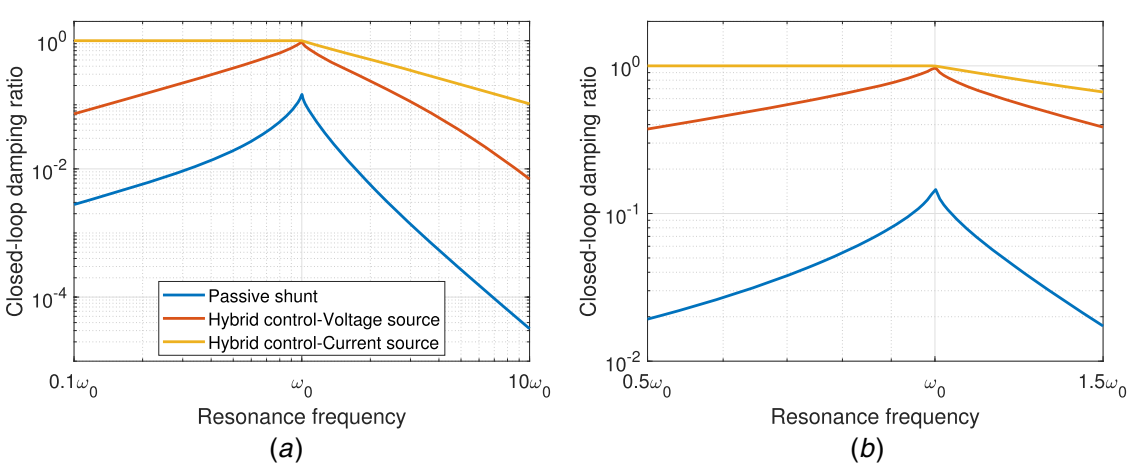

Fig. 12 (*a*) Closed-loop damping ratio versus the variation of the resonance frequency when the control parameters are kept constant and tuned to provide the critical damping for the primary system, i.e., $\omega=\omega_0$ and (*b*) details near $\omega=\omega_0$

response function from the input force disturbance to the velocity. The expressions for G_f and G_{cl} are given in Table 1. The result that is obtained in this section is based on a unit forcing amplitude.

Considering a constant value of the closed-loop damping (=0.47), Fig. 11(*a*) compares the active and reactive power for purely active control system and the hybrid control systems using active voltage source and current source, separately. The value of the closed-loop damping ratio (=0.47) is chosen arbitrary to see the general trend of the active power and the reactive power through a large frequency range. DVF is used for the purely active control system. One can be observed that the active power for all configurations is always positive through the entire frequency range. This means that the device does not deliver energy in the system and it is *hyperstable*. The reactive power for the hybrid control system when the active voltage source is applied is positive before the resonance frequency and negative after that. This shows the amount of energy exchanged between the structure and the transducer. The total of positive and negative reactive power is almost zero.

Targeting any closed-loop damping, the integral of the active power through the entire frequency range changes for any configurations. Therefore, the mean square value of the active power is considered as the performance index. It can be written as [41]:

$$E[|P_{ac}|] = \int_{-\infty}^{\infty} \frac{|f_d(\omega)|^2}{2} \left|G_f(j\omega) \times G_{cl}(j\omega) \times G_{cl}^*(j\omega)\right| d\omega \tag{26}$$

where $|f_d(\omega)|^2$ is the power spectral density of the input disturbance force. For the case of white noise excitation force, it is constant as a function of frequency as $(f_d(\omega) = f_d)$. Therefore, the mean square value of the power can be simplified as:

$$E[|P_{ac}|] = |f_d|^2 \int_{-\infty}^{\infty} \frac{1}{2} \left|G_f(j\omega) \times G_{cl}(j\omega) \times G_{cl}^*(j\omega)\right| d\omega \tag{27}$$

The normalized mean square value I is defined to represent the ratio of the active power to the excitation force with a uniform spectrum density like:

$$I = \frac{E[|P_{ac}|]}{|f_d|^2} = \int_0^{\infty} \left|G_f(j\omega) \times G_{cl}(j\omega) \times G_{cl}^*(j\omega)\right| d\omega \tag{28}$$

Figure 11(*b*) compares the performance index I as a function of the closed-loop damping ratio. One sees that the active power is zero for 16% damping ratio and below. This value of the damping is realized by the passive control system according the considered parameters of the system which is defined in Sec. 2. While there is no external power required to realize 16% damping ratio by the passive control system, a similar purely active control system requires a large amount of external power. In addition, the active power for the hybrid control systems is always less than the purely active control system. However, for high values of the closed-loop damping, the active power for the hybrid configurations is close to the active power for the purely active control system. The is because most of the work is done by the active portion of the hybrid systems.

5 Robustness Analysis

The aim of this section is to analyze the robustness of the designed hybrid control systems compared to the purely passive control system. It is particularly focused on the uncertainty of the resonant frequency. To this end, the resonance frequency of the structure changes from ten times lower value to ten times higher value than the resonance frequency of the primary system while the parameters of the controllers are kept constant. The active part of both hybrid control systems is tuned in such a way that the closed-loop system is critically damped, i.e., the closed-loop damping ratio is equal to one, for the primary system ($\omega_0 = 100$ rad/s).

Figure 12 shows the closed-loop damping ratio against the resonance frequency of the system. One sees that the performance of the passive control system degrades sharply by changing the resonance frequency of the system. The active voltage source improves the damping of the system around the primary resonance frequency. It can still provide more than 30% damping ratio in the closed-loop system for even 50% changes in the resonance frequency. Furthermore, it can be concluded from Fig. 12 that the active current source makes the system incredibly robust. If $\omega < \omega_0$, the corresponding hybrid control system can still provide critical damping in the closed-loop system. Moreover, if $\omega > \omega_0$, the control performance degrades slowly. For instance, the controlled system realizes more than 50% damping ratio when the resonance frequency is two times greater than the primary resonance frequency.

6 Conclusions

The hybridization of a passive electromagnetic shunt damper with an active control systems has been proposed and analyzed in details. The *RC* shunt has been used in series with an electromagnetic transducer as the passive control system and its parameters have been optimized based on the method of maximum damping. Both the active voltage source in series with *RC* elements and the active current source in parallel with it have been proposed for the hybrid configurations. It has been demonstrated that the system "electromagnetic device + active voltage source" can be seen as an equivalent transducer with an enhanced coupling constant T; equivalence formulae have been presented. In this case, it has been illustrated that the optimal value of the resistance R is modified to a larger value as a function of the feedback gain g_1 in order to improve the damping of the system. In addition, it has been shown that the active current source behaves like a DVF. In this case, the feedback gain g_2 has been optimized based on the method of maximum damping while there is no need to change the parameters of the passive *RC* circuit. The fact that R does not need to be changed in this configuration is a major advantage compared to the implementation of the active voltage source, as it is much easier to implement a fail-safe system. Moreover, the power consumption has been highlighted to compare the hybrid control systems and purely active control system (using DVF). As a consequence, it has been presented that both hybrid control systems can improve the control performance of the purely passive system while it has less power consumption in comparison with the purely active control system. The designed configurations reinforce the robustness of the system because they can sustain a higher level of uncertainty. In particular, the active current source makes the system significantly robust because it can realize critical damping even when the resonance frequency is lower than tuning frequency.

Acknowledgment

The authors are grateful to the financial support of MAVERIC (Wal'innov project 1610122).

Data Availability Statement

The datasets generated and supporting the findings of this article are obtainable from the corresponding author upon reasonable request. The authors attest that all data for this study are included in the paper. Data provided by a third party are listed in Acknowledgment.

References

[1] Behrens, S., Fleming, A. J., and Reza Moheimani, S. O., 2005, "Passive Vibration Control Via Electromagnetic Shunt Damping," IEEE/ASME Trans. Mech., **10**(1), pp. 118–122.

[2] Marneffe, B. De, 2007, Active and Passive Vibration Isolation and Damping Via Shunted Transducers. *These*, Faculté des Sciences Appliquées, Université Libre de Bruxelles.
[3] Inoue, T., Ishida, Y., and Sumi, M., 2008, "Vibration Suppression Using Electromagnetic Resonant Shunt Damper," ASME J. Vib. Acoust., **130**(4), p. 041003.
[4] Den Hartog, J. P., 1934, *Mechanical Vibrations*, McGraw-Hill, New York.
[5] Tang, X., Liu, Y., Cui, W., and Zuo, L., 2016, "Analytical Solutions to h_2 and h_∞ Optimizations of Resonant Shunted Electromagnetic Tuned Mass Damper and Vibration Energy Harvester," ASME J. Vib. Acoust., **138**(1), p. 011018.
[6] Zhu, S., Shen, W., and Qian, X., 2013, "Dynamic Analogy Between An Electromagnetic Shunt Damper and a Tuned Mass Damper," Smart Mater. Struct., **22**(11), p. 115018.
[7] Ormondroyd, J., and Den Hartog, J. P., 1928, "The Theory of the Dynamic Vibration Absorber," ASME J. Appl. Mech., **50**(7), pp. 9–22.
[8] McDaid, A. J., and Mace, B. R., 2013, "A Self-Tuning Electromagnetic Vibration Absorber With Adaptive Shunt Electronics," Smart Mater. Struct., **22**(10), p. 105013.
[9] McDaid, A. J, and Mace, B. R, 2016, "A Robust Adaptive Tuned Vibration Absorber Using Semi-Passive Shunt Electronics," IEEE Trans. Indus. Electron., **63**(8), pp. 5069–5077.
[10] Niederberger, D., Behrens, S., Fleming, A. J, Reza Moheimani, S. O., and Morari, M., 2006, "Adaptive Electromagnetic Shunt Damping," IEEE/ASME Trans. Mech., **11**(1), pp. 103–108.
[11] Elliott, S. J, and Zilletti, M, 2014, "Scaling of Electromagnetic Transducers for Shunt Damping and Energy Harvesting," J. Sound. Vib., **333**(8), pp. 2185–2195.
[12] Yan, B., Zhang, X., Luo, Y., Zhang, Z., Xie, S., and Zhang, Y., 2014, "Negative Impedance Shunted Electromagnetic Absorber for Broadband Absorbing: Experimental Investigation," Smart Mater. Struct., **23**(12), p. 125044.
[13] Yan, B., Wang, K., Kang, C.-X., Zhang, X.-N., and Wu, C.-Y., 2017, "Self-Sensing Electromagnetic Transducer for Vibration Control of Space Antenna Reflector," IEEE/ASME Trans. Mech., **22**(5), pp. 1944–1951.
[14] Zhou, S., Jean-Mistral, C., and Chesné, S., 2019, "Electromagnetic Shunt Damping With Negative Impedances: Optimization and Analysis," J. Sound. Vib., **445**, pp. 188–203.
[15] Yan, B., Wenguang Zheng, H. M., Jian, B., Wang, K., and Wu, C., 2019, "Nonlinear Electromagnetic Shunt Damping for Nonlinear Vibration Isolators," IEEE/ASME Trans. Mech., **24**(4), pp. 1851–1860.
[16] Yan, B., Ma, H., Zhang, L., Zheng, W., Wang, K., and Wu, C., 2020, "A Bistable Vibration Isolator With Nonlinear Electromagnetic Shunt Damping," Mech. Syst. Signal Process., **136**, p. 106504.
[17] Stabile, A., Aglietti, G. S., Richardson, G., and Smet, G., 2017, "Design and Verification of a Negative Resistance Electromagnetic Shunt Damper for Spacecraft Micro-Vibration," J. Sound. Vib., **386**, pp. 38–49.
[18] Paknejad, A., Zhao, G., Osée, M., Deraemaeker, A., Robert, F., and Collette, C., 2020, "A Novel Design of Positive Position Feedback Controller Based on Maximum Damping and h_2 Optimization," J. Vib. Control, **26**, pp. 1155–1164.
[19] Zhao, G., Paknejad, A., Raze, G., Deraemaeker, A., Kerschen, G., and Collette, C., 2019, "Nonlinear Positive Position Feedback Control for Mitigation of Nonlinear Vibrations," Mech. Syst. Signal Process., **132**, pp. 457–470.
[20] Fleming, A. J, Behrens, S., and Reza Moheimani, S. O., 2003, "Active Lqr and h_2 Shunt Control of Electromagnetic Transducers," 42nd IEEE International Conference on Decision and Control (IEEE Cat. No. 03CH37475), Vol. 3, Maui, HI, IEEE, pp. 294–2299.
[21] Fleming, A. J, Reza Moheimani, S. O., and Behrens, S., 2005, "Synthesis and Implementation of Sensor-Less Active Shunt Controllers for Electromagnetically Actuated Systems," IEEE Trans. Control Syst. Technol., **13**(2), pp. 246–261.
[22] Fleming, A. J, and Reza Moheimani, S. O., 2006, "Inertial Vibration Control Using a Shunted Electromagnetic Transducer," IEEE/ASME Trans. Mech., **11**(1), pp. 84–92.
[23] Preumont, A., 2011, *Vibration Control of Active Structures. An Introduction*, 3rd ed., Springer, Heidelberg, Germany.
[24] Collette, C., and Chesne, S., 2016, "Robust Hybrid Mass Damper," J. Sound. Vib., **375**, pp. 19–27.
[25] Chesné, S., and Collette, C., 2018, "Experimental Validation of Fail-Safe Hybrid Mass Damper," J. Vib. Control, **24**(19), pp. 4395–4406.
[26] Chesne, S., Inquieté, G, Cranga, P, Legrand, F, and Petitjean, B, 2019, "Innovative Hybrid Mass Damper for Dual-Loop Controller," Mech. Syst. Signal Process., **115**, pp. 514–523.
[27] Alujević, N., Zhao, G., Depraetere, B., Sas, P., Pluymers, B., and Desmet, W., 2014, "H2 Optimal Vibration Control Using Inertial Actuators and a Comparison With Tuned Mass Dampers," J. Sound. Vib., **333**(18), pp. 4073–4083.
[28] Agnes, G. S, 1994, "Active/passive Piezoelectric Vibration Suppression," Smart Structures and Materials 1994: Passive Damping, Vol. 2193, Orlando, FL, International Society for Optics and Photonics, pp. 24–34.
[29] Tsai, M. S., and Wang, K. W., 1999, "On the Structural Damping Characteristics of Active Piezoelectric Actuators With Passive Shunt," J. Sound. Vib., **221**(1), pp. 1–22.
[30] Tang, J, and Wang, K. W., 2001, "Active-Passive Hybrid Piezoelectric Networks for Vibration Control: Comparisons and Improvement," Smart Mater. Struct., **10**(4), p. 794.
[31] Morgan, Ronald A, and Wang, K. W., 1998, "An Integrated Active-Parametric Control Approach for Active-Passive Hybrid Piezoelectric Network With Variable Resistance," J. Intell. Mater. Syst. Struct., **9**(7), pp. 564–573.
[32] Morgan, R. A., and Wang, K. W., 2002, "An Active-Passive Piezoelectric Absorber for Structural Vibration Control Under Harmonic Excitations With Time-Varying Frequency, Part 1: Algorithm Development and Analysis," ASME J. Vib. Acoust., **124**(1), pp. 77–83.
[33] Bo Fang, MingMing Li, Cao, DengQing, and Huang, WenHu, 2013, "Modeling and Analysis of Cantilever Beam With Active-Passive Hybrid Piezoelectric Network," Sci. China Technol. Sci., **56**(9), pp. 2326–2335.
[34] Tsai, M. S., and Wang, K. W., 2002, "A Coupled Robust Control/Optimization Approach for Active-Passive Hybrid Piezoelectric Networks," Smart Mater. Struct., **11**(3), p. 389.
[35] Zhao, Y., 2010, "Vibration Suppression of a Quadrilateral Plate Using Hybrid Piezoelectric Circuits," J. Vib. Control, **16**(5), pp. 701–720.
[36] Tsai, M. S., and Wang, K. W., 1996, "Control of a Ring Structure with Multiple Active-passive Hybrid Piezoelectrical Networks," Smart Mater. Struct., **5**(5), p. 695.
[37] Hagedorn, P. and Spelsberg-Korspeter, G., eds., 2014, "Electromagnetic and Piezoelectric Transducers," *Active and Passive Vibration Control of Structures*, Darmstadt, Udine, pp. 213–248.
[38] Slotine, J.-J. E, and Li, W.,1991, *Applied Nonlinear Control*, Vol. 199, Prentice hall Englewood Cliffs, NJ.
[39] Horowitz, P., and Hill, W., 1989, *The Art of Electronics*, 2nd ed., Cambridge University Press, New York.
[40] Chesne, S, Billon, K, Collette, C, and Zhao, G, 2018, "Power Flow Analysis for Hybrid Mass Damper Design," International Design Engineering Technical Conferences and Computers and Information in Engineering Conference, Vol. 8, Quebec City, Quebec, Canada, American Society of Mechanical Engineers, pp. 1–6.
[41] Zilletti, M., Gardonio, P., and Elliott, S. J, 2014, "Optimisation of a Velocity Feedback Controller to Minimise Kinetic Energy and Maximise Power Dissipation," J. Sound. Vib., **333**(19), pp. 4405–4414.